Local-Transfer Gaussian Process (LTGP) Learning for Multi-fuel Capable Engines

Sai Ranjeet Narayanan*, Zongxuan Sun†, and Suo Yang‡
Department of Mechanical Engineering, University of Minnesota Twin Cities, Minneapolis, MN 55414, USA

John J. Miller§ and Simon Mak¶
Department of Statistical Science, Duke University, Durham, NC 27708, USA

Kenneth S. Kim‖ and Chol-Bum M. Kweon**
U.S. Army Combat Capabilities Development Command Army Research Laboratory, Aberdeen Proving Ground, MD 21005, USA

Data-driven engine surrogate models have been widely used to emulate in-cylinder trends of pressure and heat release rate for a wide variety of applications. For example, engines using multi-fuels, e.g., varying fuel cetane number (CN) or different sustainable aviation fuel (SAF) blends, require optimization of input parameters related to fuel injection and ignition assistance to achieve maximum combustion efficiency. Such an optimization task requires building an accurate surrogate model for the engine. Gaussian processes (GPs) are a popular choice: they provide accurate predictions as well as efficient uncertainty quantification to guide decision-making. One challenge, however, is the costly nature of engine combustion experiments, which results in limited data for surrogate training with many input parameters, i.e., with significant variability in engine parameters and conditions. To address this, we present a new local transfer learning Gaussian process (LTGP) surrogate, which transfers knowledge from CFD simulations to learn the expensive combustion response surface, on which limited data is available. A key novelty of the LTGP is the use of a carefully-integrated classifier that regulates when learning should be transferred using ignition misfire data from CFD simulations. Compared to the standard GP surrogate, we show that the proposed model achieves superior prediction performance for engine combustion modeling.

I. Nomenclature

ARL	=	Army Research Laboratory
$ATDC$	=	After Top Dead Center
CAD	=	Crank Angle Degrees
$CA50$	=	Crank Angle at 50% Total heat release
CN	=	Cetane Number
$EACI$	=	Energy-Assisted Compression Ignition
IAP	=	Ignition Assistant Power
MIT	=	Main Injection Timing
SAF	=	Sustainable Aviation Fuel

*Ph.D. Student, Student Member AIAA
†Frank Rowley Professor
‡Richard and Barbara Nelson Assistant Professor, suo-yang@umn.edu (Corresponding Author), Senior Member AIAA
§Ph.D. Student
¶Assistant Professor
‖Mechanical Engineer, Army Research Directorate, Member AIAA
**Program Manager, Army Research Directorate, Member AIAA

II. Introduction

Achieving multi-fuel capability for internal combustion (IC) engines is an emerging need, arising from demands for greater operational versatility and extended range for aviation applications in the industrial/commercial and military sectors. One type of IC engines, compression ignition (CI) engines, must be able to run consistently on jet fuels, even with fuel property variation present for conventional jet fuels. Understanding CI engine ignition behavior with fuel property variation and appropriate engine control becomes even more important when sustainable aviation fuels (SAF) is integrated with conventional jet-A type fuels in the commercial fuel supply for operational flexibility [1]. SAFs, such as isobutanol-derived alcohol-to-jet (ATJ), have an extremely low fuel cetane number (CN) of around 17 [2], which indicates low ignition quality. Upon blending with high CN jet-A type fuels, such as F-24 with CN 50, these fuel mixtures can exhibit a broad variation in CN from 30 to 50 [3], which poses challenges for ignition. Ignition assistants, such as glow plugs, have been tested to effectively enhance ignition in CI engines (such engines are known as energy-assisted CI or EACI engines) across a broad range of fuel CN [4–7]. In addition to changing CN and fuel properties, EACI engines must also adapt to changing ambient conditions of low temperature & pressure. This necessitates the development of robust control system models for optimizing engine performance [8–10].

Typical control system frameworks for such engines are developed based on data-driven models, such as Gaussian process (GP) regression [10, 11]. These data-driven models are usually trained using experimental data. However, there are many challenges that inhibit experimental data generation, including engine malfunctions, manufacturing delays and logistical challenges. To overcome this difficulty, well-validated physics-based computational fluid dynamics (CFD) models can be used to supplement data generation for control system training [12]. Despite their flexibility, however, CFD simulations are computationally expensive and time consuming, which again limits the quantity of generated data. Machine learning (ML) provides a promising solution for such data bottlenecks. ML has been utilized effectively to build surrogate models of IC engines, spanning from neural networks (NN) [13–15] to GPs [16–21]. GPs, in particular, have seen wide use in building IC engine surrogates. GP surrogates are appealing not only because of their excellent predictive performance [16, 22–25], but also their ability to provide efficient uncertainty quantification for timely downstream decision-making [26–28].

One critical challenge for surrogate training here, however, is the high cost of real engine combustion experiments. This is further compounded by the moderate number of control parameters required for engine combustion, which prohibits the generation of training data that sufficiently fills this parameter space. Given such limitations on training data generation from both experiments and CFD, it is essential to have a surrogate model that effectively utilizes and integrates both sources of limited data. To this end, a recent development in ML called transfer learning [29, 30] provides a promising solution for this multi-source data assimilation (DA) problem. The idea is to transfer the knowledge learned from a source system with sufficient training data, to improve performance on a target system with limited data. For example, in our study, the target system is the combustion process of a real engine (experiments), whereas the source system is the simulated combustion process via CFD. Although transfer learning has been successfully applied in various ML contexts, including image classification [31] and natural language processing [32], there has been little work investigating its use for surrogate modeling of internal combustion engines; we tackle this in the current work.

One important point of consideration when using transfer learning models is the potential for "negative transfer", where the transferred information can hurt (rather than help) the learning performance on the target system. Current works have proposed various source selection methodology to select informative sources to transfer knowledge [33, 34]. Here, in transferring information from CFD simulations to real engine experiments, one way to mitigate negative transfer is to identify when CFD ignition misfires arise over the parameter space. The proposed LTGP surrogate adopts such a strategy: it first learns a classifier on when CFD misfires arise, then fits a transfer learning model only within local regions on the parameter space where there are no misfires. In doing so, the LTGP avoids the undesirable negative transfer of information from CFD misfires for surrogate modeling of real combustion experiments, where such misfires do not arise.

The remaining of this paper proceeds as follows. Section III surveys the engine geometry and parameters used for our study, as well as the corresponding physical models used in the validated CFD case setup. The LTGP methodology is then highlighted in detail, showing how the surrogate model blends together the different levels of training data sources as well as using support vector machine (SVM) based classification of misfires (abnormal combustion points) for accurate engine CA50 predictions. Section IV reports the LTGP and standard GP predictions of CA50 and validates them with experimental "true" CA50 values. Section V concludes the paper by summarizing the research efforts and findings in this work.

III. Methodology

A. Numerical CFD model details

The system being modeled is based on an EACI engine from previous studies [4, 5, 35], as shown in Fig. 1, where the piston bowl and engine head are displayed. The fuel injector with seven nozzles is shown in Fig. 2a. The EACI engine contains a glow plug (i.e., an ignition assistant or IA) attached to the engine head, such that the tip of the glow plug is located an in-line orientation with one of the fuel nozzle spray (Fig. 2b).

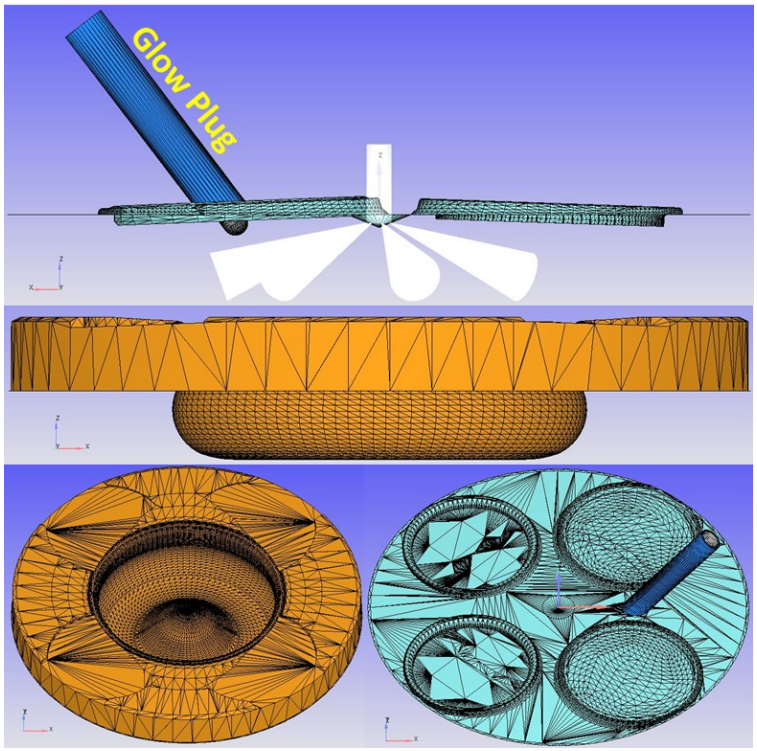

Fig. 1 CFD model geometry of the metal engine. The piston bowl (orange) and engine head (cyan) are shown, along with the glow plug (dark blue).

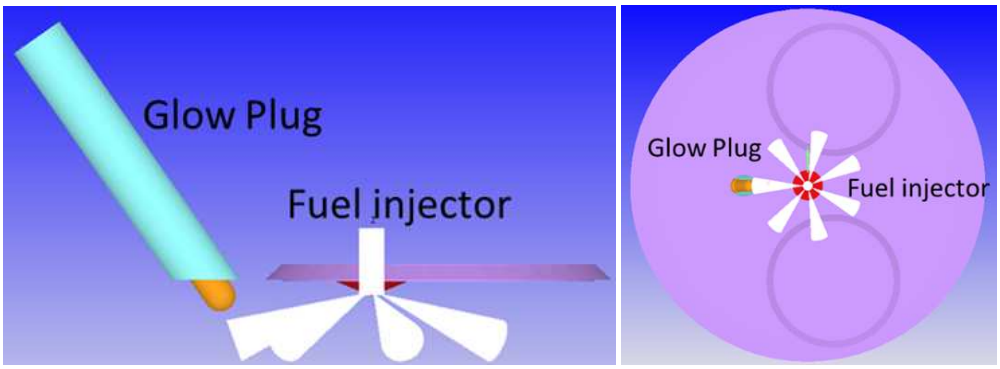

(a) Side view **(b) Bottom view**

Fig. 2 Ignition Assistant (i.e., Glow Plug) and Fuel Injector.

The closed-cycle engine simulations were conducted on Converge CFD 3.0 software [36] with a starting crank angle

of -130 CAD and ending crank angle of +130 CAD. Table 1 displays the physical model details and Table 2 displays the operating conditions and relevant engine parameters for the cases used in this work. The four control variables in this study are the Main Injection Timing (MIT, also known as Start-of-Injection, or SOI), the Ignition Assistance Power (IAP), fuel Cetane Number (CN), and Engine Speed (RPM). The different ATJ/F-24 fuel blends for varying fuel CN are represented in the simulations by a multi-component blend [37], which consists of n-decane, toluene and iso-octane as the fuel surrogate species. The CN is varied by adjusting the mass fractions of these constituents.

Table 1 Engine model details [35].

PHYSICAL MODEL	NAME
Combustion	SAGE Chemical Kinetics Solver + Three point PDF method [38]
Chemical mechanism	Multi-compoment (178 sp., 758 reactions) [37]
Turbulence model	RANS (RNG $k-\epsilon$) [39]
Droplet Evaporation model	Frossling model [40]
Spray Breakup model	KH-RT model [41]
Collision model	No-Time-Counter (NTC) collision model [42]

Table 2 Engine parameter details [35].

PARAMETER	VALUES [UNITS]
Engine speed	1200 - 2400 [rpm]
Bore	83 [mm]
Stroke	90.4 [mm]
CR Length	144.8 [mm]
Nozzle holes	7
IA Temp/Power	350 - 1400 [K]/0 - 70 [Watt]
Inj. Duration	0.66 [ms]
Inj. Mass	12 [mg]
IVC Temperature	330 [K]
IVC Pressure	88.87 [kPa]

B. Local-Transfer Gaussian Process (LTGP) model details

In our study, we are interested in the important combustion quantity CA50, the crank angle at 50% total heat release. The measurement of CA50 is expensive and time-consuming with the real engines. In comparison, a virtual CFD simulator is more cost-efficient to explore the relationship between the CA50 and control variables. Since the results of real experiments and virtual simulators are governed by the same physical laws, we can transfer information from the simulated data to the learning of the experimental data (i.e., we can utilize the trends of the experimental/real-system data to guide the control system). Sometimes, however, high quantitative deviation arises between them due to insufficient validation of the simulations with experiments, especially when a misfire phenomenon arises in the CFD simulation but not in a real engine (or vice versa). Such deviations could cause inaccurate or even incorrect predictions of the trends (e.g., opposite trends), which is not desirable. Therefore, we propose a local transfer Gaussian process modeling framework, which only leverages information from the CFD simulation to the real engine at specific regions of the parameter space.

Let $\mathbf{x} \in \mathbb{R}^4$ consists of the four control variables: RPM, CN, MIT, and IAP. The responses are CA50 (at a given combination of input parameters) for both the virtual CFD simulation and the real experimental tests. For simplicity, we denote the CFD-simulated response as a source output $f_S(\mathbf{x})$, for which a large number of simulation data are available. We then denote the real engine response as a target output $f_T(\mathbf{x})$, for which the experimental data are limited and transfer learning is desired. Suppose the responses for the simulation $\mathbf{f}_S = [y_i^S]_{i=1}^m$ are available at parameters

$\mathbf{X}_S = [\mathbf{x}_i^S]_{i=1}^m$, and the responses of the real engine $\mathbf{f}_T = [f_j^T]_{j=1}^n$ are tested at parameters $\mathbf{X}_T = [\mathbf{x}_j^T]_{j=1}^n$. Further let $\mathbf{Z}_S = \{z(\mathbf{x}) \in \{0,1\} | \mathbf{x} \in \mathbf{X}_S\}$ be the indicator for the ignition misfire in the CFD simulations: $z(\mathbf{x}_{new}) = 1$ indicates misfire; and $z(\mathbf{x}_{new}) = 0$ indicates full combustion.

The proposed transfer learning method consists of two procedures: **(1)** we first learn the distribution of ignition misfire in the parameter space and predict the misfire indicator $z(\mathbf{x}_{new})$ for the CFD simulation; **(2)** we then transfer information from the simulated response to the real response *locally*: transfer is permitted at inputs for which misfires do not happen ($z(\mathbf{x}_{new}) = 0$), while transfer is forbidden where misfire happens ($z(\mathbf{x}_{new}) = 1$). Those steps are described in detail below. In the first step, we need to learn the regions where the ignition misfire happens in the parameter space. We make use of a support vector machine (SVM) classifier with a rational quadratic kernel :

$$k_{svm}(\mathbf{x}, \mathbf{x}') = \exp\left(-\frac{\|\mathbf{x} - \mathbf{x}'\|_2}{l_{svm}}\right),$$

where l_{svm} controls the influence of each sample on the decision boundary. Such a model is trained on the misfire indication data $\mathbf{Z}_S$ from the CFD simulation. Denote the trained classifier as $\hat{z}(x) \in \{0,1\}$, and let $\hat{\mathbf{X}}_S \subset \mathbf{X}_S$ denote the subset of CFD training inputs resulting in full combustion (i.e., $z(\mathbf{x}) = 0$ for $\mathbf{x} \in \hat{\mathbf{X}}_S$).

Next, we construct a local transfer GP surrogate model that incorporates the misfire knowledge:

$$f_T(\mathbf{x}) = [1 - \hat{z}(\mathbf{x})] f_T^I(\mathbf{x}) + \hat{z}(\mathbf{x}) f_T^{II}(\mathbf{x}), \tag{1}$$

where $f_T^I(\mathbf{x})$ is a transfer model leveraging information from the CFD-simulated data $f_S(\mathbf{x})$ for the prediction of experimental response (i.e., prediction of the experimental/real-system output at $\mathbf{x}$) $f_T(\mathbf{x})$ (which will be discussed later in Eq. 2), and $f_T^{II}(\mathbf{x})$ is a no-transfer model built on the experimental data only (which will also be discussed later in Eq. 4). The key novelty here is that we control the information transfer according to the predicted class of a CFD response: if $\mathbf{x}$ is in the fully-combusted region, transfer is permitted to enhance the prediction of real engine's response; on the other hand, if the points $\mathbf{x}$ is classified into the misfire category, the simulated response shares no similarity with the real engine's response and information transfer is forbidden between them. At the points with full combustion in the CFD simulation, we adopt the following transfer model connecting the source (simulated) and the target (experimental) responses :

$$\begin{aligned} f_T^I(\mathbf{x}) &= \rho(\mathbf{x}) f_S(\mathbf{x}) + \delta(\mathbf{x}), \\ f_S(\mathbf{x}) &\sim \mathbf{GP}\{\mu_S, k_S(\cdot,\cdot)\} \\ \delta(\mathbf{x}) &\sim \mathbf{GP}\{\mu_\delta, k_\delta(\cdot,\cdot)\}. \end{aligned} \tag{2}$$

Here, the first line models the target response f_T^I as a weighted source response $f_S(\mathbf{x})$, where $\rho(\mathbf{x}) = \boldsymbol{\beta}^\top \mathbf{x}$ is the transfer weight that depends on the parameter $\mathbf{x}$. The function $\delta(\mathbf{x})$ accounts for the discrepancy between the weighted source and the target. Since neither $f_S(\mathbf{x})$ nor the $\delta(\mathbf{x})$ are known, we place independent Gaussian priors on them, where μ and $k(\cdot,\cdot)$ represent the mean and kernel function, respectively. The popular choices for the kernel functions include Gaussian and Matérn functions. In this work, we employ the widely-used Gaussian kernels for surrogate models:

$$k(\mathbf{x}, \mathbf{x}') = \sigma^2 \exp\left[-\sum_{j=1}^{4} \frac{(x_j - x_j')^2}{2l_j^2}\right], \tag{3}$$

where σ^2 is the variance parameter controlling the variation of the process and $\{l_j\}_{j=1}^4$ are the length-scales controlling the smoothness of sample paths (i.e., the individual functions that are generated when you draw a sample from the probability distribution defined by the Gaussian process). The GP mean parameters μ_S and μ_δ are set to zero, while the hyper-parameters in k_S and k_δ and the transfer weight parameter $\boldsymbol{\beta}$ are estimated through maximum likelihood methods using the fully-combusted source data $\hat{\mathbf{X}}_S$ and the target data $\mathbf{X}_T$.

Regarding the points in the misfired region, we fit a single Gaussian process model using only the target data:

$$f_T^{II}(\mathbf{x}) \sim \mathbf{GP}\{\mu_T, k_T(\cdot,\cdot)\}. \tag{4}$$

As before, the hyper-parameters in $k_T(\cdot,\cdot)$ are estimated from the experimental data. With such a no-transfer model, the misfired data in the source will not influence the target learning.

After the above transfer model f_T^I and no-transfer model f_T^{II} are trained, we predict $\hat{f}_T(\mathbf{x}_{new})$ at the new parameter $\mathbf{x}_{new}$. If the new parameter locates in a predicted fully-combusted region, i.e., $\hat{z}(\mathbf{x}_{new}) = 0$, the posterior of $\hat{f}_T(\mathbf{x}_{new})$ follows:

$$\hat{f}_T(\mathbf{x}_{new}) \sim N(\hat{\mu}_T^I(\mathbf{x}_{new}), (\hat{\sigma}_T^2)^I(\mathbf{x}_{new})), \tag{5}$$

where the posterior mean and variance are given by:

$$\hat{\mu}_T^I(\mathbf{x}_{new}) = \rho(\mathbf{x}_{new})\mu_S + \mu_\delta + (\mathbf{k}_{new}^I)^\top (\mathbf{K}^I)^{-1}\left[\begin{pmatrix}\mathbf{f}_S\\ \mathbf{f}_T\end{pmatrix} - \begin{pmatrix}\mu_S\mathbf{1}_m\\ \boldsymbol{\rho}(\mathbf{X}_T)\odot\mu_S\mathbf{1}_n + \mu_\delta\mathbf{1}_n\end{pmatrix}\right]; \tag{6}$$

$$(\hat{\sigma}_T^2)^I(\mathbf{x}_{new}) = \rho^2(\mathbf{x}_{new})k_S(\mathbf{x}_{new},\mathbf{x}_{new}) + k_\delta(\mathbf{x}_{new},\mathbf{x}_{new}) - (\mathbf{k}_{new}^I)^\top(\mathbf{K}^I)^{-1}(\mathbf{k}_{new}^I), \tag{7}$$

with $\mathbf{k}_{new}^I = [\mathbf{k}_{new}^S, \mathbf{k}_{new}^\delta]$, $\mathbf{k}_{new}^S = [k_S(\mathbf{x}_{new},\mathbf{x}_i)]_{\mathbf{x}_i\in\hat{\mathbf{X}}_S}$, $\mathbf{k}_{new}^\delta = [k_\delta(\mathbf{x}_{new},\mathbf{x}_j)]_{\mathbf{x}_j\in\mathbf{X}_T}$, and

$$\mathbf{K}^I = \begin{pmatrix}\mathbf{K}_S(\mathbf{X}_S) & \boldsymbol{\rho}(\mathbf{X}_T)\odot\mathbf{K}_S(\mathbf{X}_S,\mathbf{X}_T)\\ [\boldsymbol{\rho}(\mathbf{X}_S)\odot\mathbf{K}_S(\mathbf{X}_S,\mathbf{X}_T)]^\top & [\boldsymbol{\rho}(\mathbf{X}_T)\boldsymbol{\rho}^\top(\mathbf{X}_T)]\odot\mathbf{K}_S(\mathbf{X}_T) + \mathbf{K}_\delta(\mathbf{X}_T)\end{pmatrix}.$$

On the contrary, if the new parameter is classified as a misfired point, i.e., $z(\mathbf{x}_{new}) = 1$, the no-transfer posterior of $\hat{f}_T(\mathbf{x}_{new})$ is expressed as:

$$\hat{f}_T(\mathbf{x}_{new}) \sim N(\hat{\mu}_T^{II}(\mathbf{x}_{new}), (\hat{\sigma}_T^2)^{II}(\mathbf{x}_{new})), \tag{8}$$

with the posterior mean and variance given by:

$$\hat{\mu}_T^{II}(\mathbf{x}_{new}) = \mu_T + (\mathbf{k}_{new}^{II})^\top(\mathbf{K}^{II})^{-1}\Big[\mathbf{f}_T - \mu_T\Big], \tag{9}$$

$$(\hat{\sigma}_T^2)^{II}(\mathbf{x}_{new}) = k_T(\mathbf{x}_{new},\mathbf{x}_{new}) - (\mathbf{k}_{new}^{II})^\top(\mathbf{K}_T)^{-1}(\mathbf{k}_{new}^{II}), \tag{10}$$

where $\mathbf{k}_{new}^{II} = [k_T(\mathbf{x}_{new},\mathbf{x}_j)]_{\mathbf{x}_j\in\mathbf{X}_T}$ and $\mathbf{K}^{II} = \mathbf{K}_T(\mathbf{X}_T)$.

IV. Results and Discussion

A. Effect of varying experimental training points

Figure 3 displays the predicted CA50 vs. true CA50 comparisons between the LTGP and standard GP models. Specifically, we totally have 79 CFD-simulated samples and 39 experimental samples. We randomly select $n < 39$ experimental points for training. The LTGP model uses both the simulated samples as well as the selected experimental samples, while the standard GP model only uses the selected experimental samples. The performances are evaluated over another experimental test set of size 240 plus the experimental samples not used for training.

It is observed that the LTGP model consistently offers more accurate prediction than the standard GP, with the predicted CA50 points following the true trend line more closely. That is expected since the CFD data provides a better coverage of the input parameter space, and thus more information on the combustion process than the limited experimental data. The accuracy of both models increase with increasing the number of experimental training points, with the highest accuracy being observed in the 35 experimental training points case (Fig. 3e), and the lowest accuracy being observed in the 15 experimental training points case (Fig. 3a). It is also observed that the LTGP model offers better predictive performance in the CA50 range from 0 to 20 CAD, as seen in the green boxes. The accuracy of the model is lowered near the extreme outlier CA50 of 30 CAD and above, which are typically partial burns or misfires.

Table 3 displays the mean absolute error (MAE) across 30 different trials for each case with a certain number of experimental training points. It is seen that the MAE for the models reduce with an increase in experimental training points. The MAE for the LTGP model is consistently lower than the standard GP model, and shows a more significant decrease in MAE (from 7.16 to 3.77) than the standard GP model (from 7.39 to 5.65) with an increase in experimental training points. Our LTGP model does not have a significant advantage with 15 experimental training points, because that data set is too limited to learn an accurate transfer weight $\rho(\mathbf{x})$. As a result, the enhanced transfer learning from relatively "low" fidelity (CFD) to high fidelity (experiments) data in the training process of the model is able to achieve much more accurate predictions of CA50, when compared to standard single fidelity GP models.

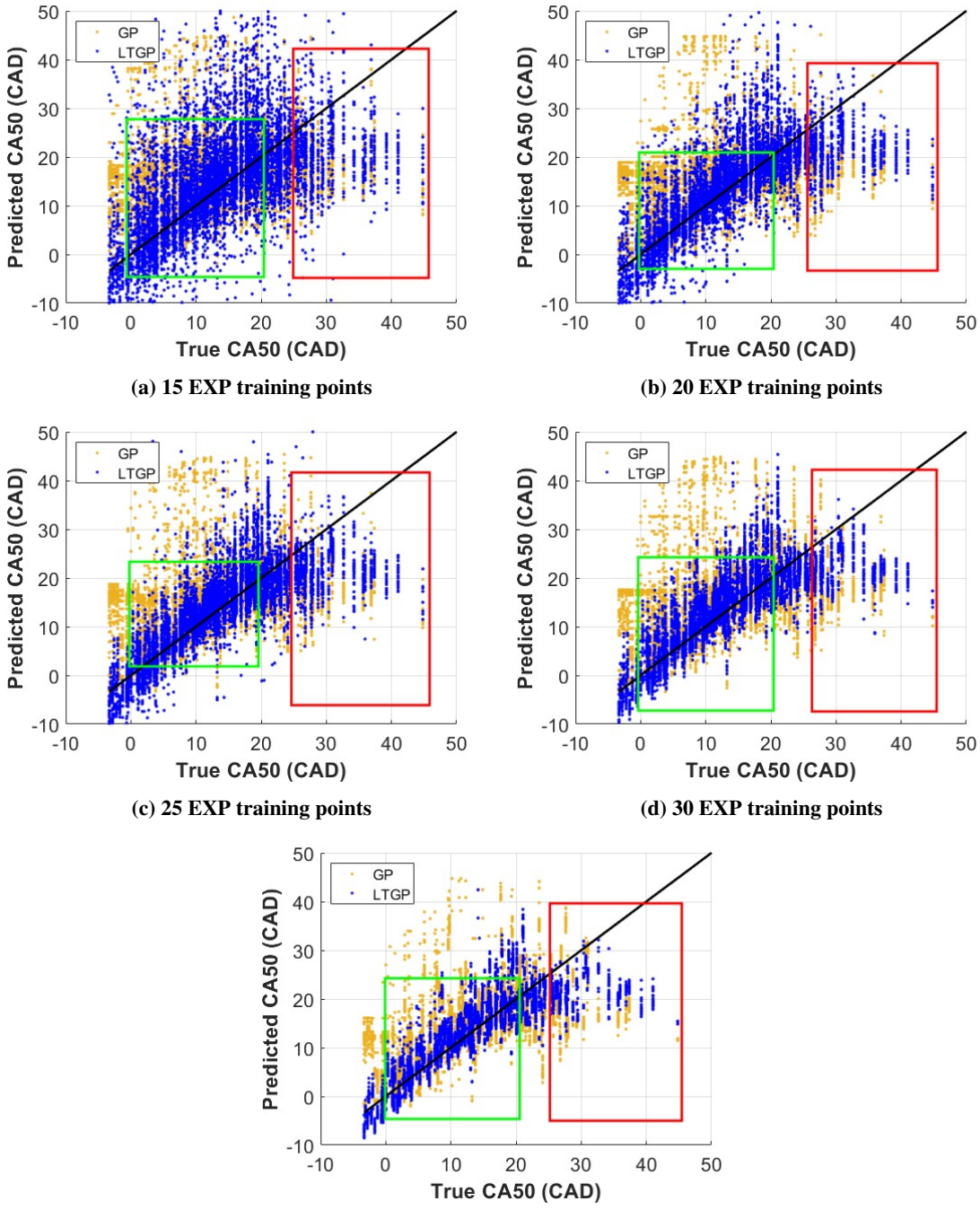

(a) 15 EXP training points

(b) 20 EXP training points

(c) 25 EXP training points

(d) 30 EXP training points

(e) 35 EXP training points

Fig. 3 Predicted CA50 vs. True CA50 for the 5 training cases classified according to the number of experimental points (EXP) used for training the LTGP model (blue) and standard GP model (GP, orange).

Table 3 Mean Absolute Error (MAE) comparison between the LTGP and standard GP models based on varying number of experimental points used in the training.

No. of EXP Points	MAE of LTGP [CAD]	MAE of standard GP [CAD]
15	7.16	7.39
20	4.75	6.52
25	4.50	6.41
30	4.09	6.39
35	3.77	5.65

B. Effect of varying RPM

After fixing the number of experimental training points as 35 based on the most accurate scenario from the previous section, we then further augment the CFD data by an additional 40 points (i.e., total of 119 points) to improve the model accuracy, which reduces the MAE of the LTGP model from 3.77 CAD to 3.34 CAD. The total number of experimental points used for validation is 230. We then analyze the error classification by the four different RPM (1200, 1500, 1800 and 2100) cases by comparing the LTGP and standard GP predictions with the experimental CA50 for different CA50 ranges, as shown in Fig. 4.

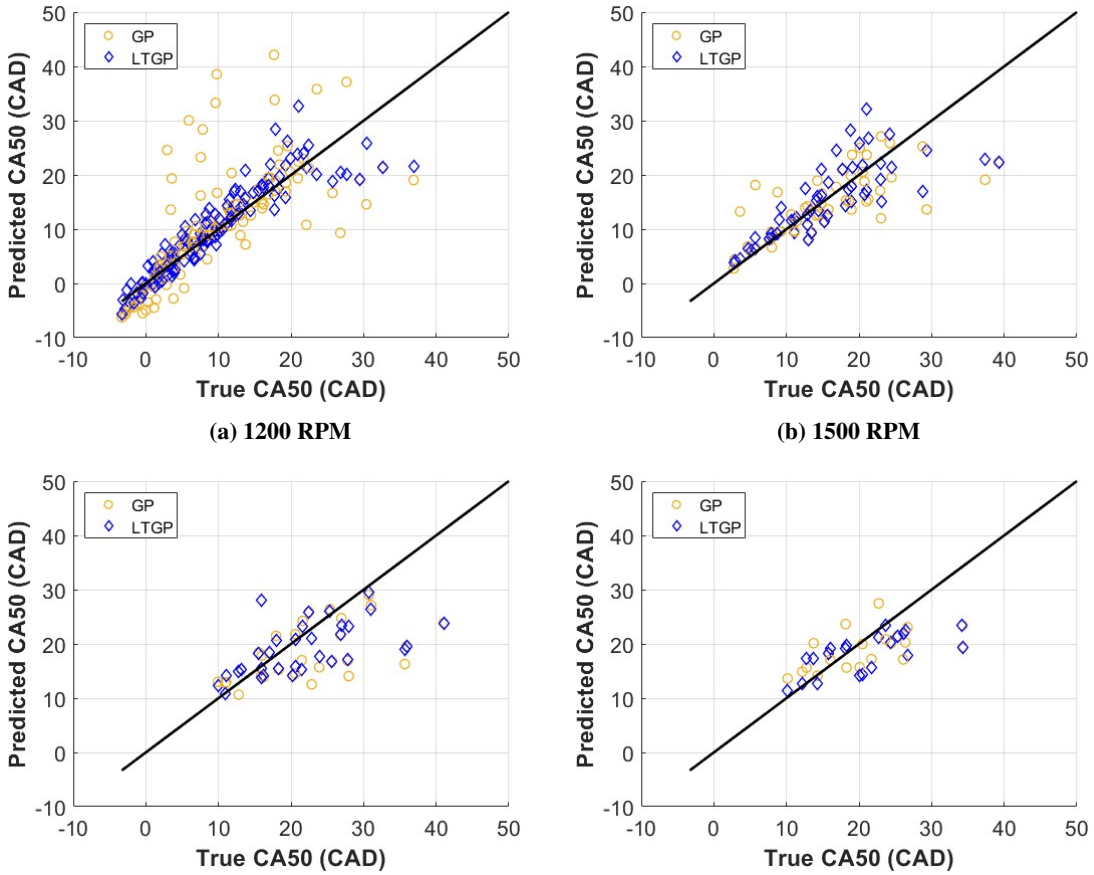

Fig. 4 Predicted CA50 vs. True CA50 for the LTGP model (blue) and standard GP model (orange) classified by varying RPM.

Table 4 Mean Absolute Error (MAE) comparison between the LTGP and standard GP models for different CA50 ranges.

CA50 range [CAD]	MAE of GP [CAD]	MAE of LTGP [CAD]	No. of Points
30 to 50	15	13	13
20 to 30	5.76	4.91	47
< 20	3.36	2.11	170
5 to 15	3.44	1.96	85
All CA50	4.51	3.34	230

Table 5 Mean Absolute Error (MAE) comparison between the LTGP and standard GP models for different RPM ranges.

RPM	MAE of standard GP [CAD] (CA50: 5 to 15 CAD)	MAE of LTGP [CAD] (CA50: 5 to 15 CAD)	No. of Points (CA50: 5 to 15 CAD)
1200	4.14	1.93	51
1500	2.29	1.95	24
1800	2.22	1.99	5
2100	3.1	2.33	5
All RPM	3.44	1.96	85

It is clear from Table 4 that the LTGP model offers higher accuracy overall compared to the standard GP model for all CA50 ranges. For instance, the LTGP model shows the highest accuracy in the CA50 range from 5 to 15 CAD (MAE around 1.96 CAD), which is much lower compared to the MAE of the standard GP model (around 3.44 CAD). The high accuracy of the LTGP model in this CA50 range is desirable, since this is the typical CA50 range used for optimizing control models [12].

Table 5 displays the MAE of the LTGP and standard GP models in the CA50 range from 5 to 15 CAD for each RPM. Starting with the 1200 RPM case which has the highest number of points available in the training and validation space, the LTGP model offers much higher accuracy (MAE = 1.93 CAD) than the standard GP model (MAE = 4.14 CAD). This can also be seen in Fig. 4a, where the LTGP CA50 agree closely with the experimental CA50 compared to the standard GP points. As the number of CFD and experimental training & validation points for 1200 RPM is more compared to other RPMs, there is a significant improvement in using the multi-fidelity LTGP model over the standard GP, which only uses 35 experimental points for training. The LTGP model offers higher accuracy for the 1500 RPM case as well, as seen in Fig. 4b. The number of CFD points used for training in the 1500 RPM case is significantly less than the number used for training in the 1200 RPM case. As a result, the gap in prediction error between the standard GP and LTGP models is smaller, although the LTGP model still offers lower MAE (MAR = 1.95 CAD) compared to the standard GP (MAE = 2.29 CAD). This trend of lower MAE for the LTGP model holds true for the 1800 RPM (Fig. 4c) and 2100 RPM (Fig. 4d) cases as well, although the number of available training & validation points for these RPMs is pretty low. Overall, the LTGP offers consistently accurate predictions compared to the standard GP model across all RPM and across all CA50 ranges.

C. Effect of varying ignition assistant power (IAP)

Figure 5 displays the prediction comparison between the LTGP and standard GP models for different IAP values. It is seen from Table 6 that the LTGP model consistently offers higher prediction accuracy than the standard GP model across all IAP values. It is seen that the highest accuracy for both models is observed at the 70 W IAP case (Fig. 5d) for the CA50 range from 5 to 15 CAD, with the LTGP model (MAE = 1.26 CAD) being more accurate than the standard GP model (MAE = 1.58 CAD). The 70 W IAP cases offer the best (most stable) combustion performance since the high temperature setting enhances ignition. Consequently, the 70 W case also has the highest number of points (both experimental and CFD) available for training and validation, followed by the 50 W case (Fig. 5c). Consequently, the models predict well for these two IAP cases. It is observed that at the 30 W case (Fig. 5b), the standard GP model

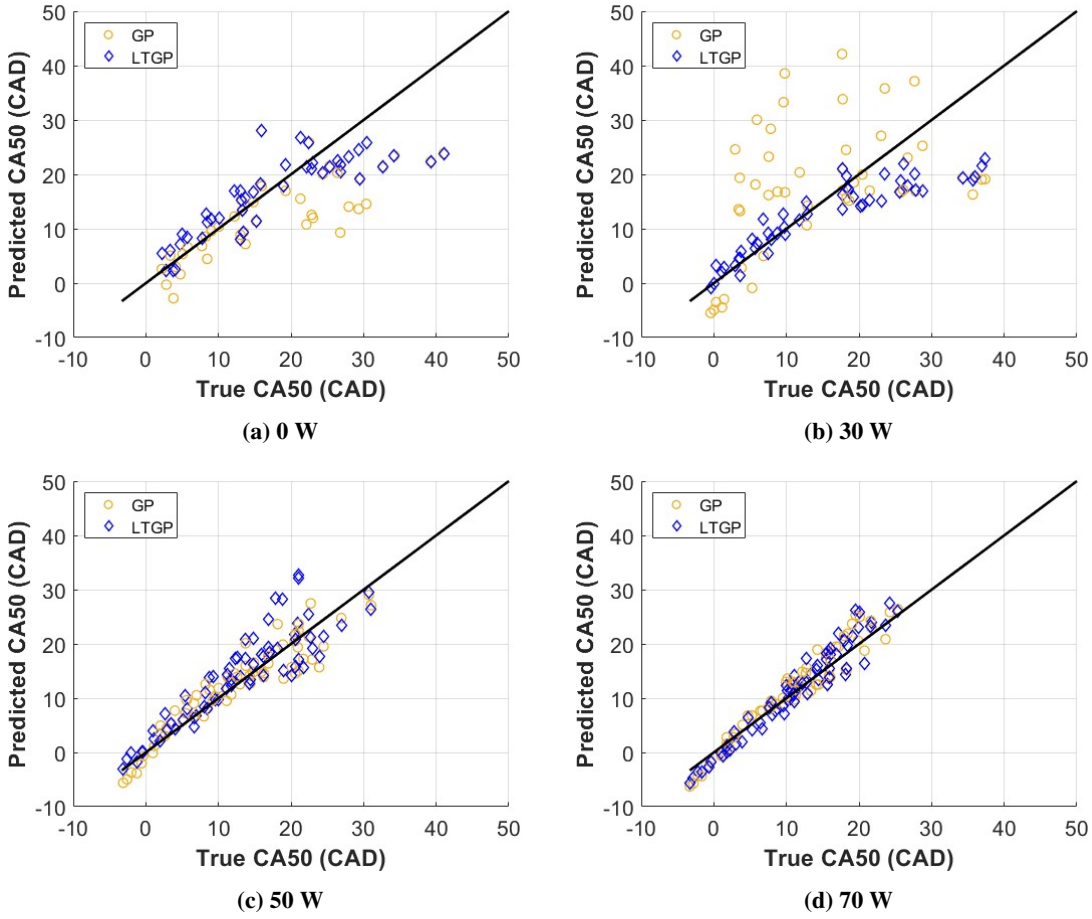

Fig. 5 Predicted CA50 vs. True CA50 for the LTGP model (blue) and standard GP model (orange), classified by varying IAP.

Table 6 Mean Absolute Error (MAE) comparison between the LTGP and standard GP models for different IAP values.

IAP [W]	MAE of GP [CAD] (CA50: 5 to 15 CAD)	MAE of LTGP [CAD] (CA50: 5 to 15 CAD)	No. of Points (CA50: 5 to 15 CAD)
0	2.25	1.96	15
30	12.06	1.50	14
50	2.06	1.80	27
70	1.58	1.26	29
All IAP	3.44	1.96	85

particularly suffers in accuracy, due to relatively sparse spread of experimental training points available at 30 W. The LTGP model, however, does not suffer from this drawback, since there were sufficient CFD points available for training in addition to experiments. As a result, the LTGP model still maintains much lower error (MAE = 1.5 CAD) compared to the standard GP (MAE = 12 CAD).

V. Conclusion

In this work, we introduce a novel local transfer Gaussian process (LTGP) method for surrogate modeling of multi-fuel capable diesel engines. The LTGP transfers the knowledge from virtual CFD simulators to real engine combustion experiments. To address the negative transfer effects caused by the misfires predicted by CFD simulation, a SVM classifier is trained to learn the local regions where transfer should be conducted. The validation results on four-dimensional combustion data demonstrate that LTGP significantly enhances the prediction accuracy of CA50 in real experiments through transferring information from simulated data, in comparison with the traditional GP models, across all CA50 ranges of interest for varying RPM and IAP.

Acknowledgments

This work is funded by the DEVCOM Army Research Laboratory (ARL) under Cooperative Agreement Number W911NF2020161, NSF CSSI 2004571, NSF DMS 2210729, NSF DMS 2316012 and DE-SC0024477. The views and conclusions contained in this document are those of the authors and should not be interpreted as representing the official policies, either expressed or implied, of the DEVCOM Army Research Laboratory or the U.S. Government. The U.S. Government is authorized to reproduce and distribute reprints for Government purposes notwithstanding any copyright notation herein. The authors would like to thank Prof. David Rothamer, Dr. Niranjan Miganakallu Narasimhamurthy, and Mr. Jacob Mathew Stafford from the Engine Research Center (ERC) at the University of Wisconsin-Madison for providing the experimental data for validation. The authors would also like to thank Prof. Sage Kokjohn, Dr. Harsh Darshan Sapra, and Dr. Randy Hessel from the University of Wisconsin-Madison for assisting with the CFD case setup. The authors would finally like to thank Convergent Science for providing CONVERGE 3.0 licenses and technical support for this work.

References

[1] Edwards, J. T., "Reference jet fuels for combustion testing," *55th AIAA aerospace sciences meeting*, 2017, p. 0146.

[2] Temme, J. E., Busch, S., Coburn, V. D., and Kweon, C.-B. M., "Fuel Blend Ratio Effects on Ignition and Early Stage Soot Formation." Tech. rep., Sandia National Lab.(SNL-CA), Livermore, CA (United States), 2019.

[3] PQIS, "Petroleum Quality Information System Annual Report 2013," , 2013.

[4] Stafford, J., Amezcua, E., Narasimhamurthy, N. M., Kim, K., Kweon, C.-B., and Rothamer, D., "Combined Impacts of Engine Speed and Fuel Reactivity on Energy-Assisted Compression-Ignition Operation with Sustainable Aviation Fuels," Tech. rep., SAE Technical Paper, 2023.

[5] Miganakallu, N., Stafford, J., Amezcua, E., Kim, K. S., Kweon, C.-B. M., and Rothamer, D. A., "Impact of Ignition Assistant on Combustion of Cetane 30 and 35 Jet-Fuel Blends in a Compression-Ignition Engine at Moderate Load and Speed," *Internal Combustion Engine Division Fall Technical Conference*, Vol. 86540, American Society of Mechanical Engineers, 2022, p. V001T03A011.

[6] Amezcua, E. R., Kim, K., Rothamer, D., and Kweon, C.-B., "Ignition Sensitivity Analysis for Energy-Assisted Compression-Ignition Operation on Jet Fuels with Varying Cetane Number," Tech. rep., SAE Technical Paper, 2022.

[7] Amezcua Cuellar, E. R., Rothamer, D., Kim, K., and Kweon, C.-B., "Optical Engine Study of Variable Energy Assisted Compression Ignition using a Glow Plug for Unmanned Aircraft Propulsion Systems," *AIAA Scitech 2020 Forum*, 2020, p. 2281.

[8] Sun, Z., and Zhu, G. G., *Design and control of automotive propulsion systems*, CRC press, 2014.

[9] Pal, A., Cornelius, A., Sun, Z., Kim, K., and Kweon, C.-B. M., "Data-driven real-time fuel cetane estimation and control design for multifuel UAVs," *Applied Energy*, Vol. 367, 2024, p. 123336.

[10] Dong, X., Goertemiller, C., Pal, A., Sun, Z., Kim, K., and Kweon, C.-B. M., "Data Driven Feedforward Control Strategy for Multi-Fuel UAS Engine," *IFAC-PapersOnLine*, Vol. 55, No. 37, 2022, pp. 627–632.

[11] Govindraju, A., Cornelius, A., Sun, Z., Kim, K., and Kweon, C.-B. M., "Rate Limited and Energy efficient Feedforward control for multi-fuel UAS engine," *ASME Letters in Dynamic Systems and Control*, 2023, pp. 1–14.

[12] Narayanan, S. R., Cornelius, A., Govind Raju, S. A., Sun, Z., Yang, S., Kim, K. S., and Kweon, C.-B. M., "Simulation-based Engine Control for an Ignition-Assisted Diesel Engine with Varying Cetane Number Fuels," *AIAA SCITECH 2024 Forum*, 2024, p. 0798.

[13] Nejadmalayeri, A., Narayanan, S. R., Yang, S., Sun, Z., Sapra, H. D., Hessel, R., Kokjohn, S., Kim, K. S., and Kweon, C.-B. M., "Multi-Fidelity Neural Network Regression for Efficient Training of Energy-Assisted Diesel Engine Control System," *Internal Combustion Engine Division Fall Technical Conference (to appear)*, Vol. 109750, American Society of Mechanical Engineers, 2023.

[14] Mishra, C., and Subbarao, P., "Machine learning integration with combustion physics to develop a composite predictive model for reactivity controlled compression ignition engine," *Journal of Energy Resources Technology*, Vol. 144, No. 4, 2022, p. 042302.

[15] Fang, X., Papaioannou, N., Leach, F., and Davy, M. H., "On the application of artificial neural networks for the prediction of NO x emissions from a high-speed direct injection diesel engine," *International Journal of Engine Research*, Vol. 22, No. 6, 2021, pp. 1808–1824.

[16] Narayanan, S. R., Ji, Y., Sapra, H. D., Kweon, C.-B. M., Kim, K. S., Sun, Z., Kokjohn, S., Mak, S., and Yang, S., "A misfire-integrated Gaussian process (MInt-GP) emulator for energy-assisted compression ignition (EACI) engines with varying cetane number jet fuels," *International Journal of Engine Research*, 2024, p. 14680874241229514.

[17] Narayanan, S. R., Ji, Y., Sapra, H. D., Yang, S., Mak, S., Sun, Z., Kokjohn, S., Kim, K., and Kweon, C. B., "Physics-integrated Segmented Gaussian Process (SegGP) learning for cost-efficient training of diesel engine control system with low cetane numbers," *AIAA SCITECH 2023 Forum*, 2023, p. 1283.

[18] Sapra, H. D., Hessel, R., Miganakallu, N., Stafford, J., Amezcua, E., Rothamer, D., Kim, K., Kweon, C.-B. M., and Kokjohn, S., "Computational Fluid Dynamics and Machine Learning-based Piston-Bowl Optimization for Energy-Assisted Compression Ignition of Low Cetane Number Sustainable Aviation Fuel Blends," *Energy Conversion and Management*, Vol. 300, 2024, p. 117929.

[19] Kavuri, C., and Kokjohn, S. L., "Exploring the potential of machine learning in reducing the computational time/expense and improving the reliability of engine optimization studies," *International Journal of Engine Research*, Vol. 21, No. 7, 2020, pp. 1251–1270.

[20] Kodavasal, J., Abdul Moiz, A., Ameen, M., and Som, S., "Using machine learning to analyze factors determining cycle-to-cycle variation in a spark-ignited gasoline engine," *Journal of Energy Resources Technology*, Vol. 140, No. 10, 2018.

[21] Ravindran, A. C., and Kokjohn, S. L., "Combining machine learning with 3D-CFD modeling for optimizing a DISI engine performance during cold-start," *Energy and AI*, Vol. 5, 2021, p. 100072.

[22] Dean, J., Corrado, G., Monga, R., Chen, K., Devin, M., Mao, M., Ranzato, M., Senior, A., Tucker, P., Yang, K., et al., "Large scale distributed deep networks," *Advances in neural information processing systems*, Vol. 25, 2012.

[23] Li, K., Mak, S., Paquet, J.-F., and Bass, S. A., "Additive Multi-Index Gaussian process modeling, with application to multi-physics surrogate modeling of the quark-gluon plasma," *arXiv preprint arXiv:2306.07299*, 2023.

[24] Li, K., and Mak, S., "ProSpar-GP: scalable Gaussian process modeling with massive non-stationary datasets," *arXiv preprint arXiv:2311.08752*, 2023.

[25] Ji, Y., Yuchi, H. S., Soeder, D., Paquet, J.-F., Bass, S. A., Joseph, V. R., Wu, C. J., and Mak, S., "Conglomerate multi-fidelity Gaussian process modeling, with application to heavy-ion collisions," *SIAM/ASA Journal on Uncertainty Quantification*, Vol. 12, No. 2, 2024, pp. 473–502.

[26] Miller, J. J., Mak, S., Sun, B., Narayanan, S. R., Yang, S., Sun, Z., Kim, K. S., and Kweon, C.-B. M., "Diverse Expected Improvement (DEI): Diverse Bayesian Optimization of Expensive Computer Simulators," *arXiv preprint arXiv:2410.01196*, 2024.

[27] Miller, J. J., and Mak, S., "Targeted Variance Reduction: Robust Bayesian Optimization of Black-Box Simulators with Noise Parameters," *arXiv preprint arXiv:2403.03816*, 2024.

[28] Chen, Z., Mak, S., and Wu, C. F. J., "A hierarchical expected improvement method for bayesian optimization," *Journal of the American Statistical Association*, Vol. 119, No. 546, 2024, pp. 1619–1632.

[29] Zhuang, F., Qi, Z., Duan, K., Xi, D., Zhu, Y., Zhu, H., Xiong, H., and He, Q., "A comprehensive survey on transfer learning," *Proceedings of the IEEE*, Vol. 109, No. 1, 2020, pp. 43–76.

[30] Wang, X., Mak, S., Miller, J., and Wu, J., "Local transfer learning Gaussian process modeling, with applications to surrogate modeling of expensive computer simulators," , 2024. URL `https://arxiv.org/abs/2410.12690`.

[31] Zhu, Y., Chen, Y., Lu, Z., Pan, S., Xue, G.-R., Yu, Y., and Yang, Q., "Heterogeneous transfer learning for image classification," *Proceedings of the AAAI Conference on Artificial Intelligence*, Vol. 25, 2011, pp. 1304–1309.

[32] Ruder, S., Peters, M. E., Swayamdipta, S., and Wolf, T., "Transfer learning in natural language processing," *Proceedings of the 2019 conference of the North American chapter of the association for computational linguistics: Tutorials*, 2019, pp. 15–18.

[33] Wang, L., Zhang, M., Jia, Z., Li, Q., Bao, C., Ma, K., Zhu, J., and Zhong, Y., "Afec: Active forgetting of negative transfer in continual learning," *Advances in Neural Information Processing Systems*, Vol. 34, 2021, pp. 22379–22391.

[34] Wang, X., Wang, C., Song, X., Kirby, L., and Wu, J., "Regularized Multi-Output Gaussian Convolution Process With Domain Adaptation," *IEEE Transactions on Pattern Analysis and Machine Intelligence*, Vol. 45, No. 5, 2022, pp. 6142–6156.

[35] Sapra, H. D., Hessel, R., Amezcua, E., Stafford, J., Miganakallu, N., Rothamer, D., Kim, K., Kweon, C.-B. M., and Kokjohn, S., "Numerical Modeling and Analysis of Energy-Assisted Compression Ignition of Varying Cetane Number Jet Fuels for High-Altitude Operation," *Journal of Engineering for Gas Turbines and Power*, 2023, pp. 1–27.

[36] Richards, K., Senecal, P., and Pomraning, E., "CONVERGE (v3. 0), Convergent Science," *Madison, WI*, 2020.

[37] Ren, S., Kokjohn, S. L., Wang, Z., Liu, H., Wang, B., and Wang, J., "A multi-component wide distillation fuel (covering gasoline, jet fuel and diesel fuel) mechanism for combustion and PAH prediction," *Fuel*, Vol. 208, 2017, pp. 447–468.

[38] Senecal, P., Pomraning, E., Richards, K., Briggs, T., Choi, C., McDavid, R., and Patterson, M., "Multi-dimensional modeling of direct-injection diesel spray liquid length and flame lift-off length using CFD and parallel detailed chemistry," *SAE transactions*, 2003, pp. 1331–1351.

[39] Tsan-Hsing, S., William, W., Aamir, S., Zhigang, Y., and Jiang, Z., "A new k-ε eddy viscosity model for high reynolds number turbulent flows," *Computers & Fluids*, Vol. 24, No. 3, 1995, pp. 227–238.

[40] Amsden, A., "A computer program for chemically reactive flows with sprays," *Report of Los Alamos National Laboratory*, 1989.

[41] Reitz, R. D., "Mechanism of breakup of round liquid jets," *Encyclopedia of fluid mechanics*, Vol. 10, 1986.

[42] Schmidt, D. P., and Rutland, C., "A new droplet collision algorithm," *Journal of Computational Physics*, Vol. 164, No. 1, 2000, pp. 62–80.